Enhanced Förster Resonance Energy Transfer on Single Metal Particle. 2. Dependence on Donor−Acceptor Separation Distance, Particle Size, and Distance from Metal Surface

ARTICLE *in* THE JOURNAL OF PHYSICAL CHEMISTRY C · AUGUST 2007

Impact Factor: 4.77 · DOI: 10.1021/jp067887r · Source: PubMed

4 AUTHORS, INCLUDING:

Yi Fu
University of Maryland, Baltimore
53 PUBLICATIONS **1,712** CITATIONS
SEE PROFILE

Joseph R Lakowicz
University of Maryland Medical Center
878 PUBLICATIONS **42,292** CITATIONS
SEE PROFILE

Published in final edited form as:
J Phys Chem C Nanomater Interfaces. 2007 August 16; 111(32): 11784–11792. doi:10.1021/jp067887r.

Enhanced Förster Resonance Energy Transfer on Single Metal Particle. 2. Dependence on Donor–Acceptor Separation Distance, Particle Size, and Distance from Metal Surface

Jian Zhang, **Yi Fu**, **Mustafa H. Chowdhury**, and **Joseph R. Lakowicz***
Center for Fluorescence Spectroscopy, Department of Biochemistry and Molecular Biology, University of Maryland School of Medicine, 725 West Lombard Street, Baltimore, Maryland 21201

Abstract

We studied the effect of metal particles on Förster resonance energy transfer (FRET) between nearby donor–acceptor pairs. The studies included the effect of donor–acceptor distance, silver particle size, and distance from the metal surface. The metal particles were synthesized with average diameters of 15, 40, and 80 nm, respectively. A Cy5-labeled oligonucleotide was chemically bound to a single silver particle with a distance of 2 or 10 nm from the surface of metal core. A Cy5.5-labeled complementary oligonucleotide was bound to the particle-conjugated oligonucleotide by hybridization. The spacer length between donor–acceptor was adjusted by the number of base pairs. FRET between the donor–acceptor pair was investigated by dual-channel single-molecule fluorescence detection. Both the emission intensities and lifetimes indicated that FRET was enhanced efficiently by the metal particles. The results showed an increase of apparent energy transfer distance with the size of silver particle and distance from the metal core. Simulations by finite-difference time-domain (FDTD) calculations were used to compare with the experimental results. The local fields at the location of the donor–acceptor pair appeared to correlate with the FRET efficiency. These results will aid in the design of metal particles for using FRET to determine biomolecule proximity at distances beyond the usual Förster distance.

Introduction

During the past several years, metal-enhanced fluorescence (MEF) has attracted considerable attention.[1-5] This interest includes studies of the underlying near-field photophysics and the use of MEF technology for high-sensitivity detection. Subwavelength metal particles are known to affect the emission of nearby fluorophores by several mechanisms including enhanced excitation, increasing the radiative decay rates, and changes in quenching.[2] Numerical calculations, such as the finite-difference time-domain (FDTD) method, can be used to simulate the electric fields near the metal particles, which are induced by the incident light.[6] However, it is more difficult to know the effects of metal particles on the emission and spectral distribution of nearby fluorophores. Therefore, it is of high interest to experimentally determine the effects of fluorophore-metal particle interaction.[7-10]

Förster resonance energy transfer (FRET) is widely used to study biomolecular structure and interactions and for numerous protein- or nucleic acid-based assays.[11] FRET occurs by the dipole–dipole interactions between an excited donor and an acceptor, and this interaction is strongly dependent on the donor–acceptor distance,[1] which is described in terms of Förster

*Corresponding author: lakowicz@cfs.umbi.umd.edu..

distance, R_0, at which FRET is 50% efficient. The Förster distance, which is usually in range of 2–6 nm, is often too short to study some large proteins, protein complexes, or moderate lengths of DNA. Hence it is of interest to identify methods to increase the FRET distances. Both theoretical and experimental results revealed that the metal particles can increase the efficiency of FRET between nearby donor–acceptor pairs,[12,13] which is accomplished by increasing the strength of the donor–acceptor interactions. We have confirmed this prediction using ensemble spectroscopy[14] and single-molecule spectroscopy (SMS).[15] However, the effects on energy transfer are not well understood. For instance, the effects of particle size and distance from the metal surface have not been reported. In this study, the donor and acceptor are attached to complementary oligonucleotides. In order to reduce the quenching by the metal particles at the excitation and emission wavelengths,[16] we used two near-infrared fluorophores, cyanines 5 (Cy5) and 5.5 (Cy5.5), as the donor and acceptor, respectively. The FRET efficiency was studied as a function of the metal particle size, the spacer length between donor and acceptor, and the distance from the donor–acceptor pair to the surface of the metal particle.

In this study, the metal particles were synthesized in a wet method by reduction of silver salt with ascorbic acid in water,[17] and the diameter of the metal core was controlled to approximately 15, 40, or 80 nm by adjusting the pH value in solution. The silver particles, which were protected by *N*-(2-mercaptopropionyl)glycine (abbreviated as tiopronin), displayed good chemical stability and solubility in water.[18] The ligand exchange reaction provides a possibility for versatile and quantitative functionalization of the organic coating layer.[19] The metal particles were succinimidylated with (2-mercaptopropionylamino)acetic acid 2,5-dioxopyrrolidin-1-yl ester via ligand exchange,[20] and then a donor-labeled single-stranded oligonucleotide was chemically bound to the single silver particle via condensation between the terminal succinimidyl ester on the silver particle and the amino moiety on the oligonucleotide (Scheme 1). Oligonucleotide **1** in Scheme 2 contains the donor, while oligonucleotide **2** or **3** contains the acceptor. The acceptor-labeled oligonucleotide was bound to the metal particle by hybridization with the bound donor-labeled oligonucleotide.[15] The donor–acceptor pair was spatially separated by the hybridized DNA duplex chain. To study the effect of distance, the spacer length between the donor and acceptor was adjusted by labeling the acceptor at different positions on the complementary oligonucleotide.

It is known that fluorescence can be quenched competitively by metals when the fluorophore is in close proximity to the metal surface. Our prior studies show that the intensity is enhanced most efficiently at distances of 10–20 nm of a fluorophore from the metal surface.[21] Hence, we attached an additional linker by a two-step surface reaction to extend the length of ligand from 2 to about 10 nm (Scheme 3), and then bound the donor–acceptor pair to the metal particle to study the influence of the linker length on the efficiency of FRET. Finally, we used finite-difference time-domain (FDTD) calculations to understand the experimental results.

Experimental Section

All reagents and spectroscopic-grade solvents were used as received from Fisher or Aldrich. RC dialysis membrane (MWCO 50 000) was obtained from Spectrum Laboratories, Inc. Nanopure water (>18.0 MΩ·cm) purified using Millipore Milli-Q gradient system, was used in all experiments. (2-Mercapto-propionylamino)acetic acid 2,5-dioxopyrrolidin-1-yl ester was synthesized as previously reported.[22] Three dye-labeled oligonucleotides (Scheme 2) were synthesized by the Biopolymer Laboratory at the University of Maryland at Baltimore, in which one is labeled by the donor Cy5 and the complementary one is labeled by the acceptor Cy5.5. Oligo **1** was also synthesized with one amino group substituted on the pyrimidine ring of a thymine base.

Preparing Succinimidylated Tiopronin-Coated Metal Nanoparticles

Tiopronin-coated silver nanoparticles were prepared by chemical reduction of silver nitrate with ascorbic acid.[23] Silver nitrate (10 mg) and 30 mg of trisodium citrate were codissolved in 50 mL of water. NaOH solution (0.1 N; 20, 100, or 500 μL) was added dropwise under stirring for 2 min. Ascorbic acid (20 mg in 10 mL of water) was then added dropwise for 5 min, and the solution was stirred for an additional 2 h. Tiopronin (20 mg in 5 mL of water) was added and the solution was stirred for 1 h at pH = 7.0. The solution was centrifuged at 8000 prm to remove the suspension. The residue was washed with water and then redispersed in 50 mL of water.

The tiopronin-coated silver particles were succinimidylated by ligand exchange (Scheme 1). (2-Mercaptopropionylamino)-acetic acid 2,5-dioxopyrrolidin-1-yl ester and tiopronin-coated silver particles were codissolved in water at a molar ratio of 1/2.[20] The solution was stirred for 24 h. Free organic components were removed thoroughly by centrifugation at 8000 prm. The residue was washed with water and then dispersed in water.

The succinimidylated ligand on the metal particle was lengthened by a two-step surface reaction. The succinimidylated metal particles were codispersed in water with an excess amount of polybis(ethylene glycol) (3-aminopropyl) (MW 1500) at a molar ratio of 1/20. The solution was stirred for 2 h, and then ammonium was added dropwise to block the terminal succinimidyl esters. The solution was removed by centrifugation at 8000 prm. The residue was washed with water and then dispersed in a water/methanol mixture (1/1 v/v). The ligands on the metal particle were succinimidylated by codissolving an excess amount of hexanedioic acid bis(*N*-succinimidyl) ester at a molar ratio of 1/20. The solution was stirred for 4 h. The suspension was removed by centrifugation at 8000 rpm. The residue was washed by methanol and water successively and then dispersed in water at pH = 7 to obtain the long-chain succinimidylated silver particles.

Binding and Hybridizing Oligonucleotides on Metal Nanoparticles

Oligo **1** was chemically bound onto the succinimidylated silver particle by condensation between the amino moiety on the oligonucleotide and the terminal succinimidyl ester moiety on the silver particle, and the acceptor-labeled complementary oligonucleotide (oligo **2** or **3**) was bound to the metal particle by hybridization with the bound oligo **1** as described in our last paper.[15]

Spectra, Förster Resonance Energy Transfer, and Transmission Electron Microscopic Measurements

Absorption spectra were monitored with a Hewlett-Packard 8453 spectrophotometer. A 650 nm filter was used to isolate the donor emission. Data were analyzed by use of a single or dual-exponential model. For SMS-FRET measurements, the coverslips (18 × 18 μm, Corning) used were first soaked in a 10:1 (v/v) mixture of concentrated H_2SO_4 and 30% H_2O_2 overnight, extensively rinsed with water, sonicated in absolute ethanol for 2 min, and dried with an air stream. Immobilization of nanoparticles on glass coverslips was achieved by adding 20 μL of 100 times diluted dye—nanoparticle suspension onto an amino-silanized coverslip, followed by spin drying at 4000 rpm. All single-molecule measurements were performed by time-resolved confocal microscopy (MicroTime 200, PicoQuant). Briefly, it consists of an inverted microscope coupled to a high-sensitivity detection setup. A single-mode pulsed laser diode (635 nm, 100 ps, 40 MHz) (PDL800, PicoQuant) was used as the excitation source. The laser power used for single-molecule experiments was maintained at 1 μW. An oil immersion objective (Olympus, 100×, 1.3NA) was employed both for focusing laser light onto the sample and for collecting fluorescence emission from the sample. The fluorescence that was transmitted through a dichroic mirror (Q655LP, Chroma) was focused onto a 75 μm pinhole

for spatial filtering to reject out-of-focus signal. The donor and acceptor emission were separated by use of a 50/50 nonpolarizing beam-splitter plate; the beams were then focused onto two single-photon avalanche diodes (SPAD) (SPCM-AQR-14, Perkin-Elmer Inc). Emission filters (Chroma HQ685/70 for the donor, HQ750/40 for the acceptor) were used to eliminate the residual excitation and to minimize spectral cross-talk. Time-dependent fluorescence data were collected with a dwell time of 50 ms. The data was stored in the time-tagged time-resolved (TTTR) mode, which allows recording of every detected photon with its individual timing information. The sum of donor counts (n_D) and acceptor counts (n_A) for each channel were used to compute an apparent FRET efficiency from the relationship $E_{app} = n_A/(n_A + \gamma n_D)$, where γ is a factor that corrects the difference in the fluorescence quantum yields of the acceptor and the donor, as well as differences in the detection efficiencies of the donor and acceptor channels of the instrument. The value of γ was estimated to be 1.4 in our experiment. In combination with a pulsed diode laser, the instrument response function (IRF) was about 200 ps fwhm (full width at half-maximum), which permits the recording of subnanosecond fluorescence lifetimes, extendable to less than 100 ps with reconvolution. Lifetimes were estimated by fitting to a reduced χ^2 value of less than 1.2 and with a residuals trace that was fully symmetrical about the zero axes.

Transmission electron micrographs (TEM) were taken with a side-entry Philips electron microscope at 120 keV. Samples were cast from water solutions onto standard carbon-coated (200–300 Å) Formvar films on copper grids (200 mesh) by placing a droplet of a 1 mg/mL aqueous sample solution on grids. The size distribution of metal core was analyzed with Scion Image Beta Release 2; at least 200 particles were counted.

Finite-Difference Time-Domain Calculations

The FDTD technique is an implementation of Maxwells's time-dependent curl equations for solving the temporal variation of electromagnetic waves within a finite space that contains a target of arbitrary shape. FDTD is now the start-of-the-art method for solving Maxwell's equations for complex geometries.[24-37] Being a direct time and space solution, FDTD offers the user a unique insight into all types of problems in photonics. Furthermore, FDTD can also be used to obtain the frequency solution by exploiting Fourier transforms, thus enabling a full range of useful quantities such as the complex Poynting vector and the transmission/reflection of light, in addition to fields around particles to be calculated.

Our FDTD calculations were performed using the program FDTD Solutions (Version 5.0) purchased from Lumerical Solutions, Inc. (Vancouver, Canada). The calculations were performed with the parallel FDTD option on a Dell Precision PWS690 workstation with the following components: dual quad-core Intel Xeon E5320 processors at 1.86 GHz, and 8 GB of RAM. All postprocessing of FDTD data was performed with MATLAB (version 7.0) purchased from Mathworks (Natick, MA). In order to maintain the accuracy and stability of the FDTD calculations, the smallest grid size to accurately model the prescribed system without being computationally prohibitive was obtained in an iterative fashion (convergence testing). In our implementation of FDTD, convergence testing was done by starting the first calculation with a grid size of $\lambda_0/20$, where λ_0 is the smallest wavelength expected in the simulation, and then reducing the grid size by half in sequential simulations and comparing the results of the calculations. The reduction of the grid size was stopped when we approached a grid size (Δ) where results closely match with the set of results that are obtained from half that particular grid size ($\Delta/2$).[36] The numerical implementation of Maxwell's equations in the FDTD algorithm requires that the time increment Δt have a specific bound relative to the spatial discretization Δ (as mentioned above) to ensure the stability of the time-stepping algorithm. In FDTD Solutions, the time step of the simulation is determined by the values of the spatial grid to ensure numerical stability and the user has the flexibility to set the total time of the

simulation in femtoseconds.[37] Typically our simulations ranged around 300 fs. Thus, all the simulations in this study had in excess of 500 000 time steps. In our implementation of FDTD, there are frequency-domain monitors that perform discrete Fourier transforms of the time-domain fields while the simulation is running. In this manner, continuous wave (CW) information is obtained at any prespecified wavelengths for the various field components (E_x, E_y, E_z, H_x, H_y, and H_z). Additionally, time domain monitors are present that provide time-domain information for the various field components within the FDTD simulation region over the entire course of the simulation. At the end of the simulation, the various field components are checked to see if they decay toward zero, thus indicating that the simulation has run for a sufficiently long time for the CW information obtained by Fourier transformations to be valid.[37]

Results and Discussion

Tiopronin-coated silver particles were synthesized with different colors from yellow to purple by decreasing the amount of base in the reaction mixture. The absorbance spectra displayed typical plasmon absorbances at 400, 430, and 570 nm (Figure 1), with simultaneous broadening of band, corresponding to larger particles.[23] The TEM images show that the average diameters of metal cores are 15, 40, and 80 nm (insets of Figure 1). The small particles of 15 and 40 nm appeared to be approximately homogeneous in size distribution but the large particles appeared to be heterogeneous. Their *average* chemical composition were estimated to be ca. (Ag) 1×10^5 and (Tio) 3×10^3; (Ag) 2×10^6 and (Tio) 2×10^4; and (Ag) 2×10^7 and (Tio) 8×10^4, respectively. These metal particles were found to display good stability in surface reactions and good solubility in water.

According to the report from Murray and co-workers,[19] ligand exchange occurs at a 1:1 molar ratio. In order to avoid multifunctionalization, the molar ratio of succinimidyl ligand/ metal particle was controlled to be 0.5. So the *average* number of terminal succinimidyl ligands per particle is 0.5 or less, even if all succinimidyl ligands are completely bound to the metal particles. It means that only half the metal particles are succinimidylated by one functionalized ligand. The low content of succinimidylation guarantees that a single oligonucleotide (Scheme 1) is bound to a silver particle.

The surface reactions can occur on the ligand of metal particles.[38] In order to study the dependence of FRET on the linker length from the metal surface, the succinimidyl ligand was lengthened by a two-step surface reaction on the particle surface. First, the terminal succinimidyl ester was chemically bound by poly(ethylene glycol) bis(3-aminopropyl) (MW 1500). Because the diamine compound was present in 20-fold excess, the metal particles were not observed to aggregate seriously by cross-linking. Then the metal particles were terminally succinimidylated by condensation with a large excess of hexanedioic acid bis(*N*-succinimidyl) ester. No aggregation of the metal particles was observed, indicating no significant cross-linking. Because only small quantities of terminal-functionalized moieties were involved in the surface reactions, it was difficult to evaluate the extent of reaction accurately by the regular method. In order to verify the occurrence of these surface reactions, we synthesized silver particles (average diameter = 15 nm) with a compact succinimidyl ester coating in deuterium water. Poly-(ethylene glycol) bis(3-aminopropyl) were covalently bound as described above. After removal of the unbound compound, the suspension was treated with NaCN to remove the metal cores. The residuals in solution were evaluated by ^{1}H NMR. There was an obvious peak of chemical shift at 3.5 ppm, indicating that the diamine compound was indeed attached to the metal particle. This result shows that the surface reaction occurs on the surface of the metal particles. In addition, we also utilized the metal particle in solution in parallel experiments without reactive chemicals as the controls. The treatments cannot alter the FRET behavior significantly, which is attributed only to the change of linker length from the metal particle.

The absorbance spectrum is not altered significantly with the surface reaction because so few reactive ligands are involved.

The animated oligonucleotide (oligo **1** in Scheme 2) was chemically bound to the metal particle with an average diameter of 15 nm via condensation between the succinimidyl ester moieties on the metal particles and the amino moieties on the oligonucleotides. Acceptor-labeled oligonucleotides (oligo **2** or **3**) were bound to the metal particles by hybridization with the bound oligo **1** in 50 mM phosphate-buffered saline (PBS) solution at pH = 7.2.[15,39] The number of dye-labeled oligonucleotide on the metal particle was analyzed quantitatively by dissolving the metal core with several drops of 0.1 N NaCN aqueous solution. The released dye-labeled oligonucleotides displayed an emission spectrum identical to that of free oligonucleotide pair, and the concentration was estimated by the emission intensity. It is inferred that the molar ratio of dye-labeled oligonucleotide/metal particle is near 1/3, indicating that the metal particle contains one or less bound donor–acceptor pair.

Because the carboxylic ligands on the metal particle were depronated in the neutral buffer solution, the oligonucleotide ligands that are negatively charged could not be physically absorbed onto the surfaces of particles. Hence, the oligonucleotides were expected to behave as if they were free in solution. The donor Cy5 displayed an emission maximum at 661 nm, while the acceptor Cy5.5 displayed a maximum at 702 nm. After binding of the oligonucleotide to the metal particle, the emission wavelength was slightly altered to 662 and 700 nm. In a typical SMD experiment, we recorded the intensity images of the donors and the acceptors simultaneously, which was accomplished by use of two detection channels and appropriate emission filters. Upon excitation with the 635 nm laser source, the fluorescent spots observed in the donor channel (inset of Figure 2A) were accompanied with the relatively weak spots in the acceptor channel (inset of Figure 2B). There was a considerable amount of cross-talk between the channels due to the spectral overlap of the two fluorophores. The intensities of individual spots can be utilized to estimate the FRET efficiency. Representative examples of the time traces were collected in the donor and acceptor channels in the absence of a metal particle (Figure 2A,B). The sudden drop in the emission intensity is due to the photobleaching of fluorophores but is not relevant to FRET efficiency. After binding of the donor–acceptor pair to the 15 nm diameter single silver particle, the intensity in the donor channel was shown to decrease (Figure 3c) while the intensity in the acceptor channel increased (Figure 3d). Control experiments showed that the light scattering from the metal particle was too weak to significantly influence the signal from the fluorophores. We collected at least 50 individual images for each sample to analyze the overall properties. Although most labeled metal particles were bound by z single D–A pair, there was a small fraction of multilabeled silver particles. The multilabeled particles did not display single-step photobleaching but multiple steps or a direct decay, so they were excluded from the analysis. It is very important to employ this kind of treatment in the count events for the analysis of only the metal particles that were bound by a single D–A pair. Histograms of the efficiencies for both long and short donor–acceptor pairs were presented in Figure 3a (oligo **1**–**2**) and Figure 4a (oligo **1**–**3**), which were shown to be centered at 0.22 and 0.06 (Table 1), respectively. Histograms of the transfer efficiencies showed dramatic increases from 0.22 to 0.55 for oligo **1**–**2** and from 0.06 to 0.38 for oligo **1**–**3** (Figure 3) when bound to the 15-nm silver particles. Additionally, it was observed that the photostability of D–A pair increased from 7 s in free state to 28 s when bound to the 15-nm silver particles, an increase of approximately 5-fold. An analogous increase was also observed in the emission enhancement on the metal substrate.[40]

The absorption maxima of Cy5 and Cy5.5 are at 610 and 650 nm, respectively. Hence, it is possible to excite Cy5 and Cy5.5 simultaneously, with the excitation source of 630 nm. Because the excitation and emission wavelengths for Cy5 and Cy5.5 show only a 40-nm separation, their efficiency for metal-enhanced fluorescence is expected to be close to each other, according

to our previous results.[42] However, the results in this case reveal that the intensity of single-molecule images for Cy5 is not altered significantly on the metal particles, but the intensity for Cy5.5 is increased 9-fold (Figure 2), indicating that the change of image is principally due to metal enhanced FRET. The efficiency of energy transfer was estimated from the total photons in the donor and acceptor channels for each individual fluorescence spot. A correction factor was used for the alignment of detectors and cross-talk between the detection channels.[40b,42]

The transfer efficiencies can be used to calculate the ratio of Förster distance over the distance between the donor–acceptor by[1]

$$\frac{R_0}{r}=\left(\frac{1}{E}-1\right)^{-1/6} \quad (1)$$

where E is the efficiency of energy transfer, R_0 is the Förster distance at which 50% energy is transferred, and r is the distance between the donor–acceptor. It is likely that the donor-to-acceptor distance remains the same for the free and particle-bound DNA. Hence the changes in the ratio (R_0/r) calculated from the transfer efficiencies represent changes in the apparent values of R_0 due to the influence of the metal particles. These ratios are shown in Figure 4b for short-chain oligo **1**–**2** and in Figure 5b for long-chain oligo **1**–**3**. For the more closely spaced D–A pair of oligo **1**–**2**, the ratio (R_0/r) increases from 0.81 for the free oligonucleotide to 1.03 for the particle-bound oligonucleotide (Figure 3b), an increase of 27%. If the value of R_0 was 8.1 nm in the absence of metal, then R_0 is increased to 11 nm due to the nearby metal particle. A similar calculation can be performed for the widely spaced D–A pair on oligo **1**–**3**. In this case, the transfer efficiencies increase from 0.06 to 0.38 (Figure 4a). This change corresponds to an increase in the ratio (R_0/r) from 0.63 to 0.92, an increase of 45% (Figure 4b).

Next we studied the effect of particle size on the FRET efficiencies. The silver particles were synthesized with average diameters of 15, 40, and 80 nm. The terminal succinimidyl ester ligand was controlled to be on average less than one on one metal particle in the ligand exchange reaction. Oligo **1** was covalently bound to the metal particle and the long-chain oligo **3** was bound by its hybridization with the conjugated oligo **1**. The energy transfer efficiencies were estimated on the basis of the number of photons detected in the donor and acceptor channels. These efficiencies were 0.38, 0.59, and 0.67, respectively, for 15-, 40-, and 80-nm silver particles (Figure 4a). These transfer efficiencies correspond to the ratio (R_0/r) of 0.92, 1.06, and 1.13 for the 15-, 40-, and 80-nm metal particles (Figure 4b), respectively. If we recall that the ratio (R_0/r) was 0.63 for free oligo **1**–**3**, the apparent values of R_0 increase by 75% for oligo **1**–**3** near the large 80 nm particle. The metal-enhanced FRET is shown to increase with increasing size of metal particle. This conclusion is consistent with the experimental and theoretical results showing stronger near-field intensity around larger metal particles.[20] Here it appears that the metal-enhanced fluorescence and metal-enhanced FRET depend on similar electromagnetic interaction between the fluorophore and the metal and that a large metal particle can result in a more efficient coupling with a fluorophore.

It is known that the interaction between the fluorophore and metal particle is strongly influenced by the distance between them.[2a] A short distance can result in a quenching of fluorophore, but a very long distance will result in a weak interaction. All above FRET results were measured when the donor–acceptor pair was bound by a 2-nm linker to the metal surface. In this next set of studies, we extended the linker length from the donor–acceptor pair to the metal particle in a two-step surface reaction as described above. Because the backbone of poly(ethylene glycol) is flexible, the spacer length is not accurately known. We feel that the negative charges on both the particle and the DNA will result in the DNA staying distant from the metal surface. The

overall length of this linker is estimated to be about 10 nm. Oligo **1** was covalently bound to the metal particle, and long-chain complementary oligo **3** was bound by the hybridization. The donor–acceptor energy transfer efficiency was observed to increase from 0.38 to 0.59 with lengthening of the linker (Figure 5a). Hence, the ratio (R_0/r) increases from 0.92 with the shorter linker to 1.06 with the longer linker (Figure 5b).

The quenching of fluorophore by the metal particle can influence the FRET between the donor and acceptor pair nearby, especially when the pair is in close proximity to the surface of metal core. However, the influence by the metal quenching is not considered because both the donor and acceptor are affected to the same extent when they are localized near the metal core. This is true especially when the excitation and emission wavelengths of donor and acceptor are close. In addition, although it is 2 nm from the connection point of oligonucleotide to the metal particle, the distance from donor or acceptor to the surface of metal core is around 5 nm. This distance is not ideal for efficient energy transfer from the fluorophore to the metal particle. Hence the quenching effect by the metal core can be expected to be weak relative to FRET between donor–acceptor pairs near the metal particle.

Metal-enhanced fluorescence is influenced by the near-field interaction of the fluorophore with the metal particle. FRET occurs by dipole–dipole interactions between an excited donor and an acceptor, so we suggest that metal-enhanced FRET is also due to near-field interaction of the D–A pair with the electric fields near the metal particle. Although a direct correlation is uncertain, we can infer that the efficiency of enhanced FRET may be strongly dependent on the distribution of the local electric field near the metal particle. The electric field distribution near the silver particles can be accurately calculated by the FDTD technique, demonstrating that the different-sized silver particles provide different distributions of the electric field under incident light at 635 nm (Figure 6). Our calculations show that the fields around the particle get more intense as well as extend further out from the particle as the particle size gets larger. Generally an intense field is expected to cause strong enhancements in fluorescence, and a weak field is expected to cause low or no enhancements in fluorescence. Using a similar analogy, we can speculate that larger particles will have a greater influence on FRET efficiency than smaller particles. Our SMD results discussed above demonstrate that the FRET efficiency increases with particle size. Hence the results of our FDTD calculations are in qualitative agreement with our experimental results. We know that, in metal-enhanced fluorescence, an optimal distance exists between the fluorophore and the surface of metal core to maximize the fluorescence enhancement. An analogous situation is also observed for metal-enhanced FRET. We can see that the enhancement in FRET efficiency of the D–A pair at 10 nm from the surface of metal core is higher than that at 2 nm, which we believe is too close to metal core.

Metal particles can affect the intrinsic decay rates of fluorophores,[2] which is observed by the lifetime decay of the donor (Figure 7). The lifetime of free oligo **1** was 2.4 ns, and it shortened to 2.1 ns when hybridized with oligo **2** and 2.2 ns when hybridized with oligo **3**. The FRET efficiencies estimated by the lifetime changes were 0.13 for oligo **1**–**2** and 0.08 for oligo **1**–**3**, close to those calculated from the intensity changes. These data reveal that the lifetime can approximately reflect the FRET interactions between the donor and acceptor. The lifetime of oligo **1**–**3** was shortened to 0.4 and 0.3 ns when bound to the 40 and 80 nm silver particles, respectively, indicating that particle size can significantly influence the coupling of the fluorophore to the metal particle.

Summary

In this paper, we studied systemically the effects of metal particle size, spacer distance between the donor and acceptor, and linker length of the donor–acceptor pair from the metal particle on metal-enhanced FRET. Two near-infrared fluorophores, Cy5 and Cy5.5, were employed as

donor and acceptor, respectively. The silver particles were synthesized with core sizes of 15, 40, and 80 nm. The donor-labeled oligonucleotide was bound to the silver particle by condensation between the amino moiety on the oligonucleotide and the terminal succinimidyl ester on the silver particle. The acceptor-labeled complementary oligonucleotide was conjugated to the bound oligonucleotide by hybridization. The donor/acceptor pair was separated by the hybridized DNA duplex. The linker from the terminated succinimidyl ester to the silver surface was lengthened from 2 to 10 nm by a two-step reaction on the surface of metal particle. The FRET efficiency was observed to depend on the oligonucleotide length that separated the donor and acceptor, the size of metal particle, and the distance from the metal surface. The increase of apparent distance (R_0/r) was dependent on the size of metal particle and the distance from the metal surface. These results are similar to the metal-enhanced fluorescence intensity. FDTD calculations were used to describe the local electric field near the different-sized silver particles under the incident light. The metal-enhanced FRET was discussed in terms of the near-field interactions of donor–acceptor pair with the local electric field. This model can be applied in optimizing metal-enhanced FRET over longer distances, especially for the detection of large biological molecules.

Acknowledgments

This research was supported by a grant from NIH, HG-02655, NCRR, and RR-08119.

References and Notes

1. Lakowicz, JR. Principles of Fluorescence Spectroscopy. Vol. 3rd ed.. Kluwer Academic/Plenum Publishers; New York: 2006.
2. (a) Lakowicz JR. Anal. Biochem 2005;337:171. [PubMed: 15691498] (b) Lakowicz JR. Anal. Biochem 2001;298:1. [PubMed: 11673890]
3. Gryczynski I, Malicka J, Shen YB, Gryczynski Z, Lakowicz JR. J. Phys. Chem. B 2002;106:2191. (b) Aslan K, Huang J, Wilson GM, Geddes CD. J. Am. Chem. Soc 2006;128:4206. [PubMed: 16568977]
4. (a) Shen Y, Swiatkiewicz J, Lin T-C, Markowicz P, Prasad PN. J. Phys. Chem. B 2002;106:4040. (b) Lee I-YS, Suzuki H, Ito K, Yasuda Y. J. Phys. Chem. B 2004;108:19368. (c) Yonzon CR, Jeoung E, Zou S, Schatz GC, Mrksich M, Van Duyne RP. J. Am. Chem. Soc 2004;126:12669. [PubMed: 15453801] (d) Song J-H, Atay T, Shi S, Urabe H, Nurmikko AV. Nano Lett 2005;5:1557. [PubMed: 16089488] (e) Kawasaki M, Mine S. J. Phys. Chem. B 2005;109:17254. [PubMed: 16853202]
5. (a) Yu F, Persson B, Lofas S, Knoll W. J. Am. Chem. Soc 2004;126:8902. [PubMed: 15264814] (b) Ekgasit S, Thammacharoen C, Yu F, Knoll W. Anal. Chem 2004;76:2210. [PubMed: 15080730] (c) Baluschev S, Yu F, Miteva T, Ahl S, Yasuda A, Nelles G, Knoll W, Wegner G. Nano Lett 2005;5:2482. [PubMed: 16351199]
6. (a) Futamata M, Maruyama Y, Ishikawa M. J. Phys. Chem. B 2003;107:7607. (b) Sherry LJ, Chang S-H, Schatz GC, Van Duyne RP, Wiley BJ, Xia Y. Nano Lett 2005;5:2034. [PubMed: 16218733] (c) Oubre C, Nordlander P. J. Phys. Chem. B 2005;109:10042. [PubMed: 16852215] (d) Wang H, Goodrich GP, Tam F, Oubre C, Nordlander P, Halas NJ. J. Phys. Chem. B 2005;109:11083. [PubMed: 16852350]
7. (a) Sokolov K, Chumanov G, Cotton TM. Anal. Chem 1998;70:3898. [PubMed: 9751028] (b) Tarcha PJ, De Saja-Gonzalez J, Rodriguez-Llorente S, Aroca R. Appl. Spectrosc 1999;53:43. (c) De Saja-Gonzalez J, Aroca R, Nagao Y, De Saja JA. Spectrochim. Acta A 1997;53:173.
8. (a) Kummerlen J, Leitner A, Brunner H, Aussenegg FR, Wokaun A. Mol. Phys 1993;80:1031. (b) Antunes PA, Constantino CJL, Aroca RF, Duff J. Langmuir 2001;17:2958. (c) Kamat PV. J. Phys. Chem. B 2002;106:7729. (c) Kelly KL, Coronado E, Zhao LL, Schatz GC. J. Phys. Chem. B 2003;107:668. (d) Hao E, Li S, Bailey RC, Zou S, Schatz GC, Hupp JT. J. Phys. Chem. B 2004;108:1224.
9. (a) Kumbhar AS, Kinnan MK, Chumanov G. J. Am. Chem. Soc 2005;127:12444. [PubMed: 16144364] (b) Bruzzone S, Malvaldi M, Arrighini GP, Guidotti C. J. Phys. Chem. B 2005;109:3807. [PubMed: 16851429] (c) Hubert C, Rumyantseva A, Lerondel G, Grand J, Kostcheev S, Billot L, Vial A, Bachelot

R, Royer P, Chang S.-h. Gray SK, Wiederrecht GP, Schatz GC. Nano Lett 2005;5:615. [PubMed: 15826096] (d) Millstone JE, Park S, Shuford KL, Qin L, Schatz GC, Mirkin CA. J. Am. Chem. Soc 2005;127:5312. [PubMed: 15826156]

10. (a) Tews KH. J. Lumin 1974;9:223. (b) Chance RR, Prock A, Silbey R. J. Chem. Phys 1974;60:2744. (c) Persson BNJ. J. Phys. C: Solid State Phys 1978;11:4251. (d) Gersten J, Nitzan A. J. Chem. Phys 1981;75:1139. (e) Ruppin R. J. Chem. Phys 1982;76:1681. (f) Barnes WL. J. Modern Opt 1998;45:661.
11. Lakowicz, JR. Emerging biomedical application of time-resolved florescence spectroscopy. In: Lakowicz, JR., editor. Topics in Fluorescence spectroscopy, Vol. 4, Probe Design and Chemical Sensing. Plenum Press; New York: 1994.
12. (a) Citrin DS. Nano Lett 2004;4:1561. (b) Citrin DS. Nano Lett 2005;5:985. [PubMed: 15884907]
13. (a) Hua XM, Gersten JI, Nitzan A. J. Chem. Phys 1985;83:3650. (b) Gersten JI, Nitzan A. Chem. Phys. Lett 1984;104:31.
14. (a) Malicka J, Gryczynski I, Fang J, Kusba J, Lakowicz JR. Anal. Biochem 2003;315:160. [PubMed: 12689825] (b) Lakowicz JR, Kusba J, Shen Y, Malicka J, D'Auria S, Gryczynski Z, Gryczynski I. J. Fluoresc 2003;13:69.
15. Zhang J, Fu Y, Lakowicz JR. J. Chem. Phys. B 2007;111:50.
16. Aguila A, Murray RW. Langmuir 2000;16:5949.
17. (a) Chen S, Wang ZL, Ballato J, Foulger SH, Carroll DL. J. Am. Chem. Soc 2003;125:16186. [PubMed: 14692749] (b) Nikoobakht B, El-Sayed MA. Chem. Mater 2003;15:1957. (c) Orendorff CJ, Murphy CJ. J. Phys. Chem. B 2006;110:3990. [PubMed: 16509687]
18. (a) Huang T, Murray RW. Langmuir 2002;18:7077. (b) Huang T, Murray RW. J. Phys. Chem. B 2001;105:12498.
19. (a) Templeton AC, Wuelfing WP, Murray RW. Acc. Chem. Res 2000;33:27. [PubMed: 10639073] (b) Ingram RS, Hostetler MJ, Murray RW. J. Am. Chem. Soc 1997;119:9175.
20. Zhang J, Malicka J, Gryczynski I, Lakowicz JR. J. Phys. Chem. B 2005;109:7643. [PubMed: 16851886]
21. (a) Drexhage KH. J. Lumin 1970;12:693.(b) Drexhage, KH. Progress in Optics XII. Wolf, E., editor. North Holland; Amsterdam: 1974.
22. Zhang J, Roll D, Geddes CD, Lakowicz JR. J. Phys. Chem. B 2004;108:12210.
23. (a) Hayat, MA., editor. Colloidal Gold: Principles, Methods, and Applications. Academic Press; San Diego, CA: 1991. (b) Feldheim, DL.; Foss, CA. Metal Nanoparticles. Synthesis, Characterization and Applications. Marcel Dekker, Inc.; New York: 2002.
24. Taflove, A.; Hagness, SC. Computational Electrodynamics: The Finite-Difference Time-Domain Method. Artech House; Boston: 2000.
25. Yee KS. Numerical solution of initial boundary value problems involving Maxwell's equations in isotropic media. IEEE Trans. Antennas Propag 1966;AP-14:302–307.
26. Yang P, Liou NK. J. Opt. Soc. Am. A 1995;12:162.
27. Yang P, Liou NK. J. Opt. Soc. Am. A 1996;13:2072.
28. Gray SK, Kupka T. Phys. Rev. B 2003;68:045415.
29. Chang S-H, Gray SK, Schatz GC. Opt. Express 2005;13:3150. [PubMed: 19495214]
30. Prather DW, Shi S. J. Opt. Soc. Am. A 1999;16:1131.
31. Maier SA, Kik PG, Atwater HA. Appl. Phys. Lett 2002;81:1714.
32. Shao DB, Chen SC. Opt. Express 2005;13:6964. [PubMed: 19498717]
33. Guiffaunt G, Mahdjoubi K. IEEE Trans. Antennas Propag 2001;43:94.
34. Sullivan, DM. Electromagnetic simulation using the FDTD method. IEEE Press; New York: 2000.
35. Berenger JP. J. Comput. Phys 1994;114:185.
36. Teflove A, Brodwin ME. IEEE Trans. Microwave Theory Tech 1975;23:623.
37. Reference Guide for FDTD Solutions. 2007. Release 5.0http://www.lumerical.com/fdtd.
38. (a) Templeton AC, Hostetler MJ, Warmoth EK, Chen S, Hartshorn CM, Krishnamurthy VM, Forbes MDE, Murray RW. J. Am. Chem. Soc 1998;120:4845. (b) Templeton AC, Hostetler MJ, Kraft CT, Murray RW. J. Am. Chem. Soc 1998;120:1906.

39. (a) Rosi NL, Mirkin CA. Chem. Rev 2005;105:1547. [PubMed: 15826019] (b) Wabuyele MB, Vo-Dinh T. Anal. Biochem 2003;77:7810.

40. (a) Fu Y, Lakowicz JR. Anal. Chem 2006;78:6238. [PubMed: 16944907] (b) Fu Y, Lakowicz JR. J. Phys. Chem. B 2006;110:22557. [PubMed: 17092001]

41. Zhang J, Matveeva E, Gryczynski I, Leonenko Z, Lakowicz JR. J. Phys. Chem. B 2005;109:7969. [PubMed: 16851931]

42. (a) Bemey C, Danuser G. Biophys. J 2003;84:3992. [PubMed: 12770904] (b) Ha T, Enderle Th. Ogletree DF, Chemla DS, Selvin PR, Weiss S. Proc. Natl. Acad. Sci. U.S.A 1996;12:6264. [PubMed: 8692803] (c) Koberling F. FRET Analysis of Free Diffusing Molecules using the MicroTime 200. 2004;(6)PicoQuant GmbH

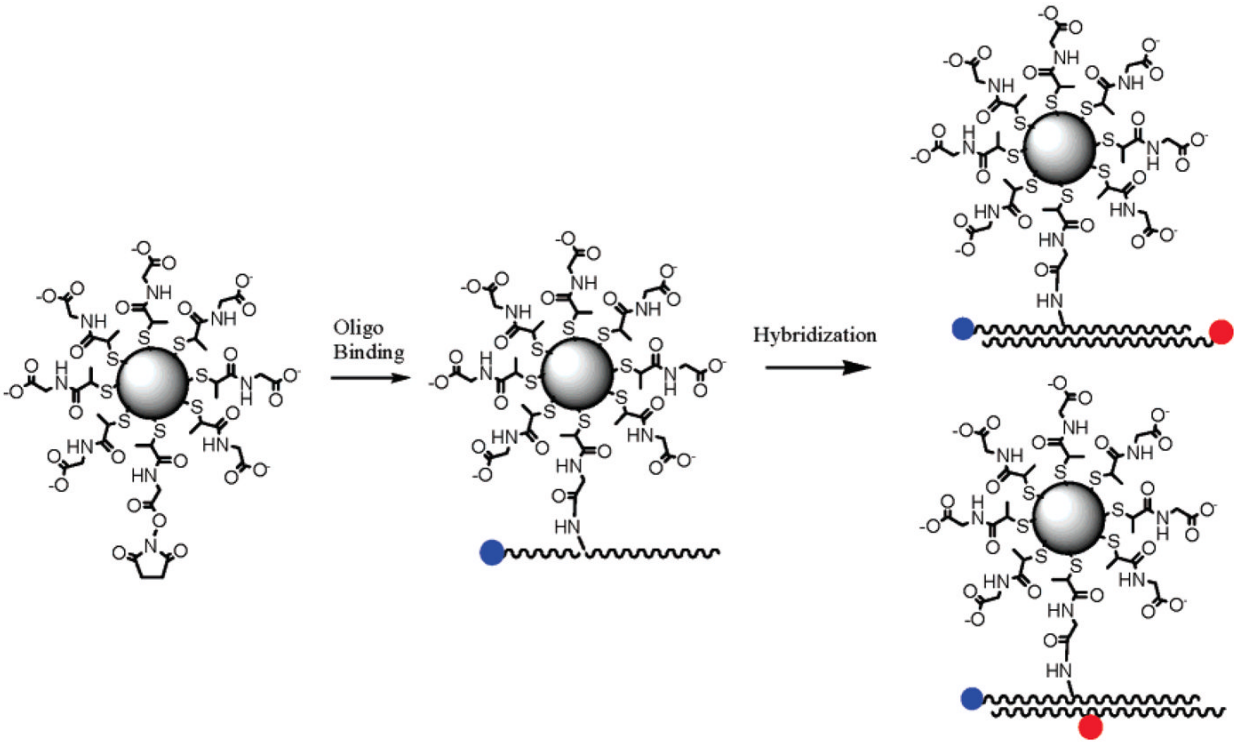

SCHEME 1.

Succinimidylated Silver Particle, Covalently Bound with Aminated Donor-Labeled Oligonucleotide and Then Conjugated with Complementary Acceptor-Labeled Oligonucleotide

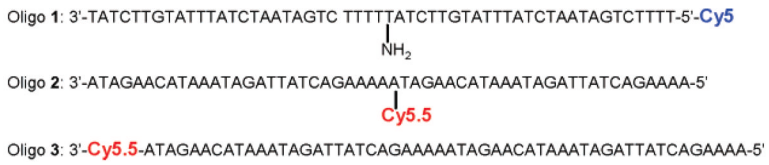

SCHEME 2.

Oligonucleotide Sequences Used in the Experiments

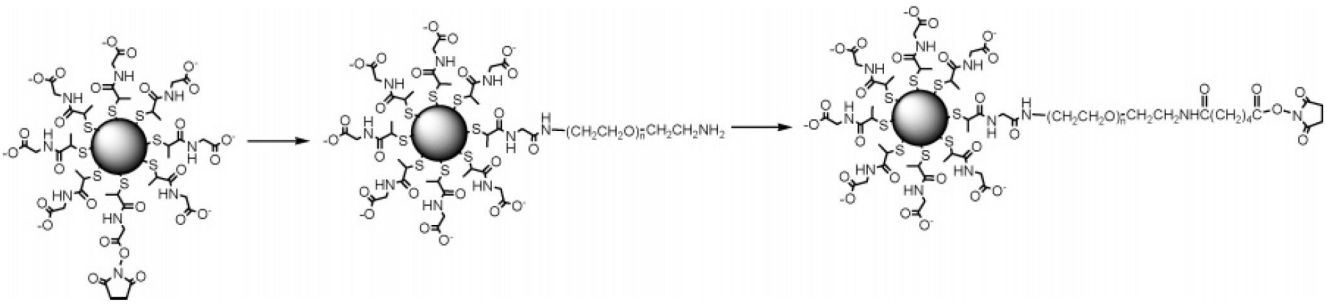

SCHEME 3.
Two-Step Reaction on the Metal Particle to Extend the Linker Length

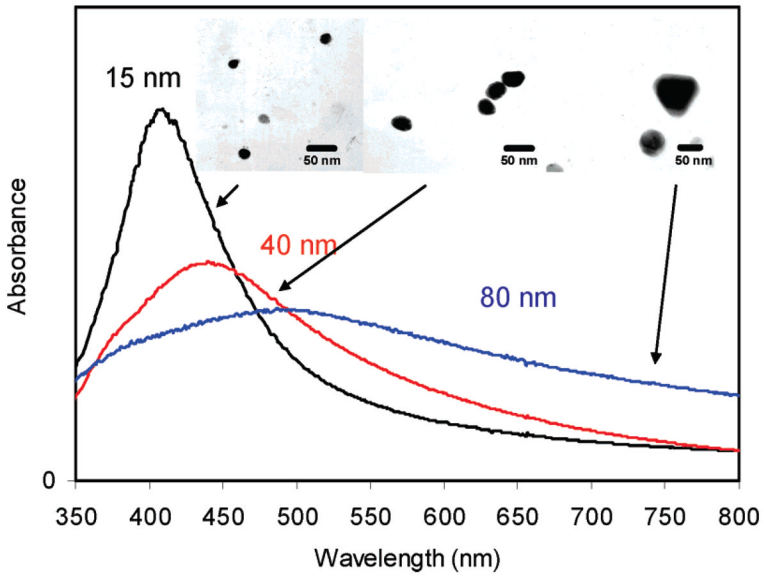

Figure 1.
Absorbance spectra of tiopronin-coated silver particles of silver particles with different core sizes, 15, 40, and 80 nm, and their corresponding transmission electron micrograph (TEM) images.

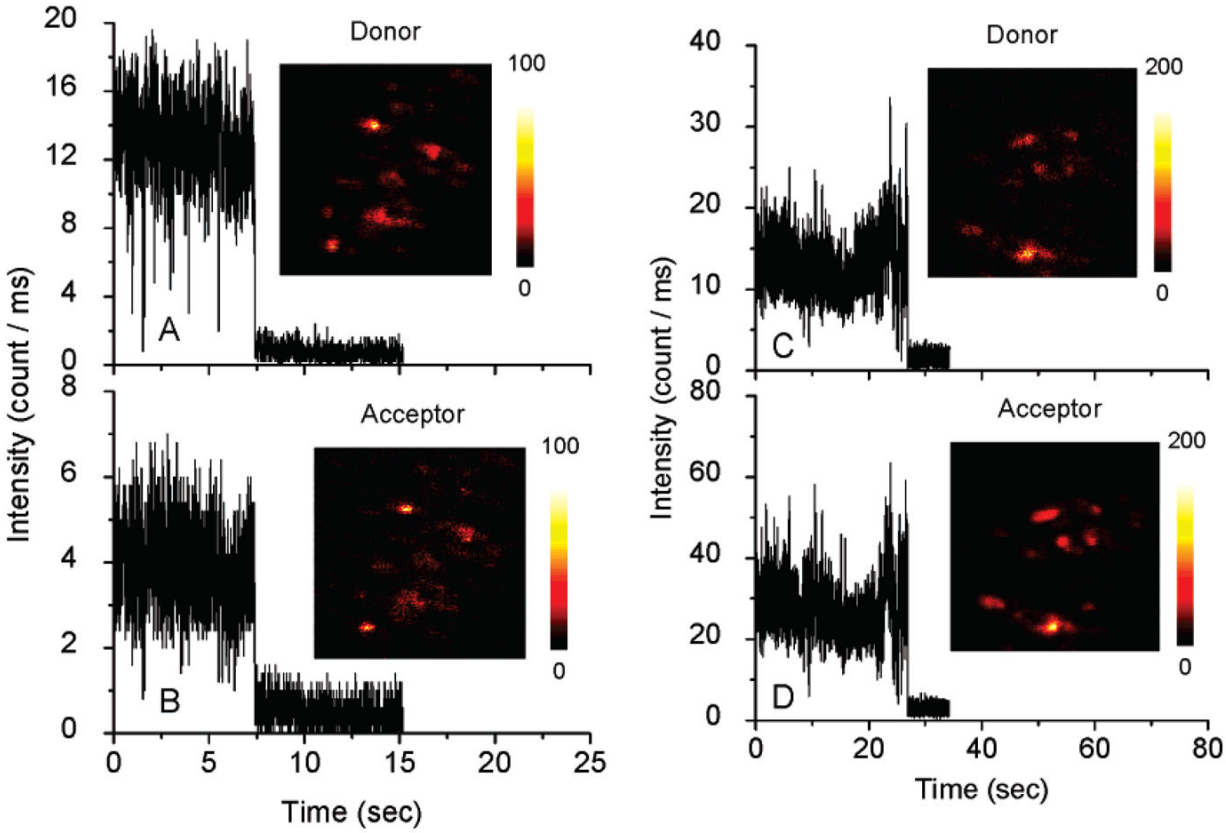

Figure 2.

Respective time-trace intensities of a free donor–acceptor pair, as seen in (a) the donor channel or (b) the acceptor channel, and a donor–acceptor pair bound on the silver particle with a diameter of 15 nm, as seen in (c) the donor channel or (d) the acceptor channel. (Insets) Respective fluorescence images. The images are 150 × 150 pixels, with an integration time of 0.6 ms/pixel. Both images were recorded simultaneously with two SPAD detectors.

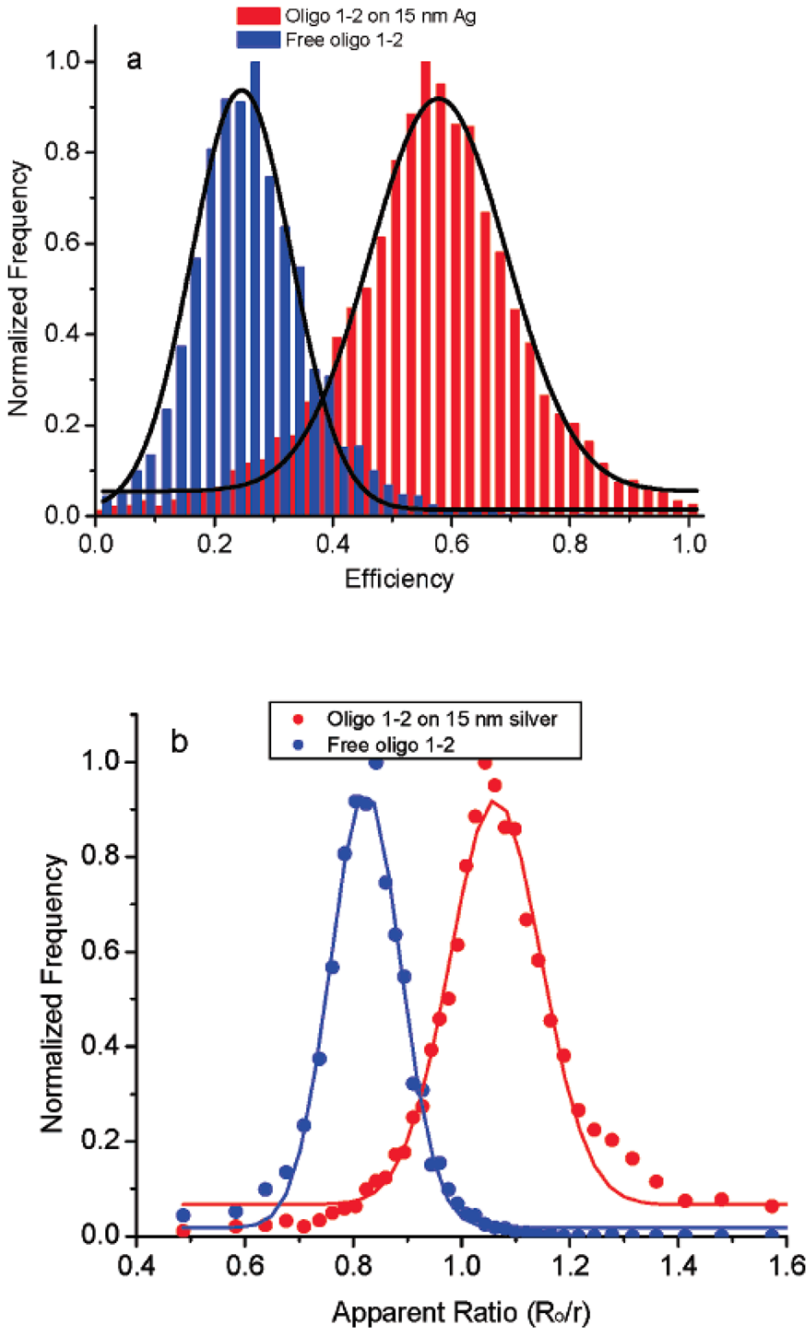

Figure 3.
Histograms of FRET on the free oligo **1**–**2** pairs and those bound to 15-nm silver particles by 2-nm linkers: (a) efficiency and (b) relative distance, counting from more than 50 single time traces.

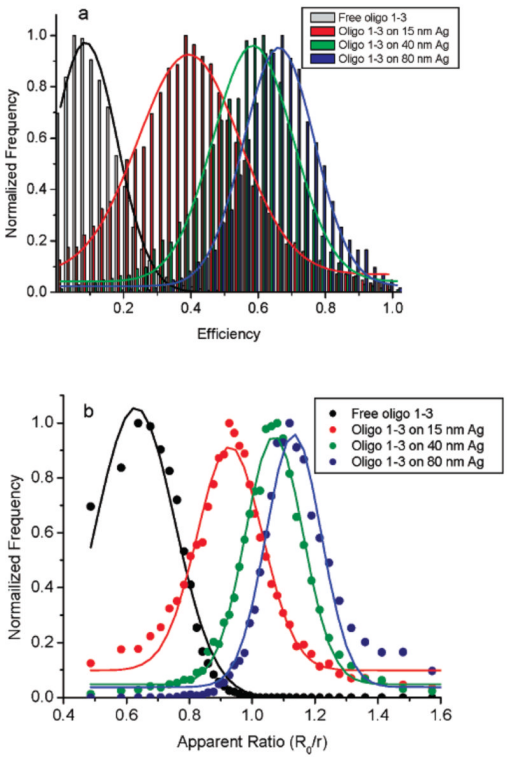

Figure 4.
Histograms of FRET on the free oligo **1**–**3** pairs and those bound to 15-, 40-, and 80-nm silver particles by 2-nm linkers: (a) efficiency and (b) relative distance, counting from more than 50 single time traces.

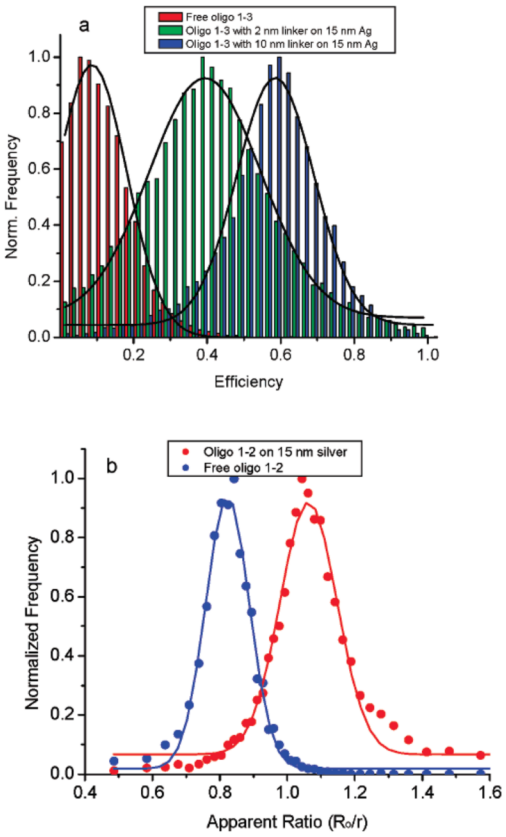

Figure 5.
Histograms of FRET on the free oligo **1**–**3** pairs and those bound to 15-nm silver particles by 2- and 10-nm linkers: (a) efficiency and (b) relative distance, counting from more than 50 single time traces.

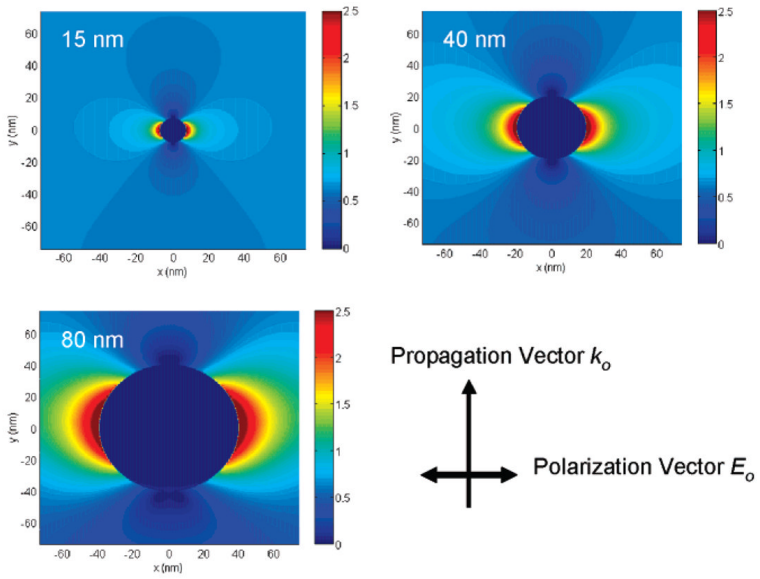

Figure 6.
Electric field intensity distribution near silver particles with different core sizes of 15, 40, and 80 nm. The field images were achieved by FDTD calculations.

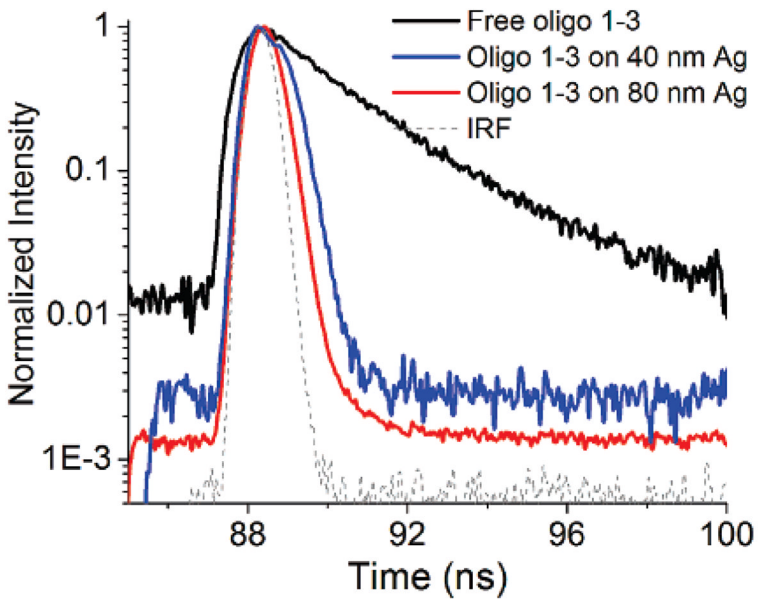

Figure 7.
Donor decay curves for the free oligonucleotide or the oligonucleotide bound on different size silver particles by 2-nm linker.

TABLE 1

Summary of FRET Data for the Cy5- and Cy5.5-Labeled Oligonucleotides

oligo	energy transfer efficiency	apparent ratio (R_0/r)
1–**2**	0.22	0.81
1–**3**	0.06	0.63
1–**2** on 15-nm Ag	0.55	1.03
1–**3** on 15-nm Ag	0.38	0.92
1–**3** on 40-nm Ag	0.58	1.06
1–**3** on 80-nm Ag	0.67	1.13
1–**3** on 15-nm Ag with 10-nm linker	0.59	1.06